Sustainable Chemical Engineering
http://ojs.wiserpub.com/index.php/SCE/

UNIVERSAL WISER PUBLISHER

Research Article

Anticorrosion and Supercapacitor Applications of Polypyrrole Coated Graphite Nanocomposites

Madhusudhan C. K.[1*], Muhammad Faisal[2], Maruthi N.[3], Narasimha Raghavendra[4], Mahendra K.[5], Abdul Kadar C. H.[2,6], Vasantha V. T.[7]

[1]Department of Physics, Vemana Institute of Technology, Koramangala, Bangalore-560034, Karnataka, India
[2]Research Centre-Physics, Department of Science and Humanities, PES University-Electronic City Campus Bangalore-560100, Karnataka, India
[3]Department of Physics, Faculty of Engineering and Technology, Jain University, Bangalore-562112, Karnataka, India
[4]Department of Chemistry, PC Jabin Science college, Hubli-580031, Karnataka, India
[5]Department of Physics, REVA University, Bengaluru, Karnataka-560064, India
[6]Department of Physics, The Oxford College of Engineering, Bommanahalli, Bangalore, 560068, India
[7]Department of Chemistry, Vemana Institute of Technology, Koramangala, Bangalore-560034, Karnataka, India
E-mail: madhuck.1990@gmail.com

Received: 29 August 2023; **Revised:** 13 October 2023; **Accepted:** 16 October 2023

Graphical abstract:

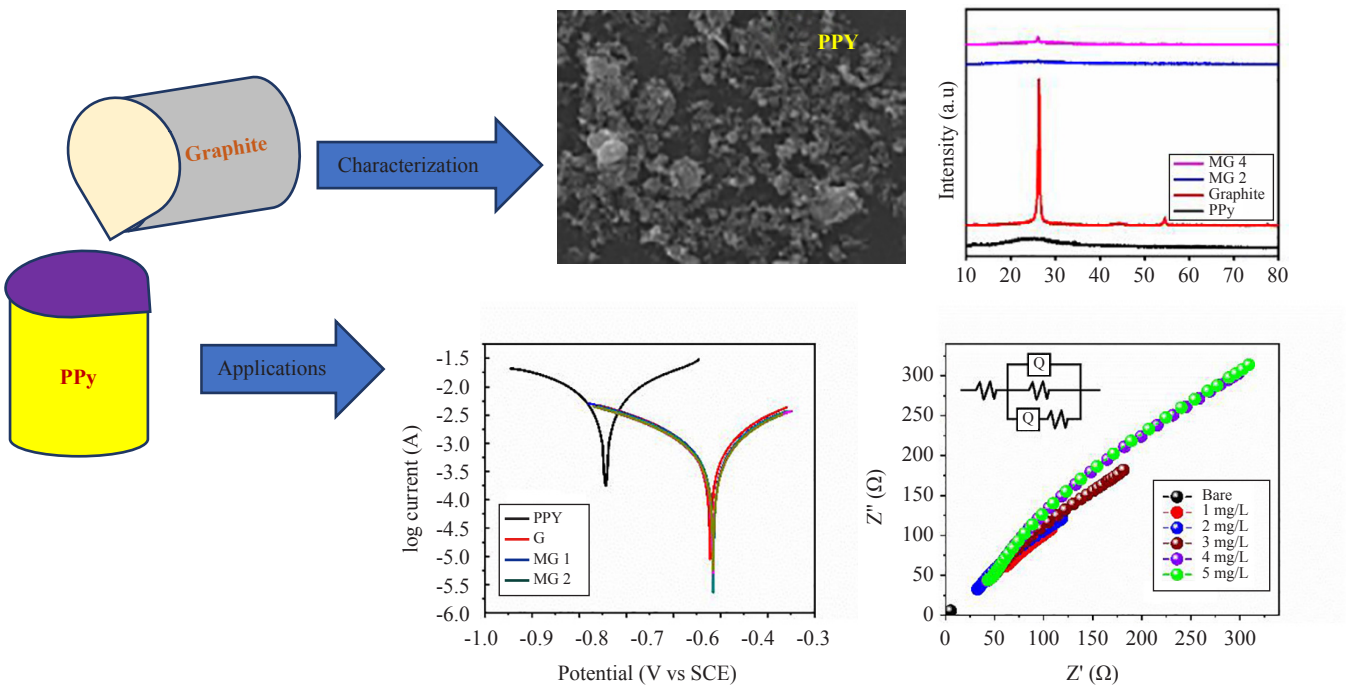

DOI: https://doi.org/10.37256/sce.5120243591

Abstract: The present investigation reports the successful incorporation of Graphite into the PPy matrix via a chemical in-situ polymerization technique. Obtained composites were thoroughly studied by using powder X-ray diffraction (PXRD), scanning electron microscopy (SEM) and Fourier transform infrared spectroscopy (FT-IR). The corrosion inhibition response of the composites on mild steel (MS), treated in acid media was analysed through atomic absorption spectroscopy (AAS), impedance, Tafel diagram (potentiodynamic polarization) and scanning electron microscopy (SEM) techniques. The results have revealed better inhibitory properties of these composites in the premeditated acid media. The Tafel and impedance curves revealed the dependency of polymer compounds on the corrosion protection of MS steel. The surface of MS is examined through the SEM technique (before and after corrosion). The synthesized materials were further studied for supercapacitor applications using electrochemical Cyclic Voltammetry (CV) and Galvanostatic Charging and Discharging studies (GCD) measurements. The supercapacitor and corrosion properties can be further optimized to develop effective PPy/G structures.

***Keywords*:** polymer nanocomposite, atomic absorption spectroscopy (AAS), tafel diagram, supercapacitor, cyclic voltammetry

1. Introduction

The rising usage of cellular phone devices with the emergence of the Internet of Things (IoT) produced a rebellion in the design and manufacture of flexible and smart electronic tools. It is necessary to explore cost-effective and versatile electrical and semiconducting hybrids capable of exhibiting the broadest range of property responses useful for the optimization of wearable devices, sensors, solar panels, screens, etc. The power supplies (batteries and supercapacitors (SCs)) for such technologies must, among other things, fit the mechanical characteristics of the wearable devices.[1] Supercapacitors are one of the prospective candidates for electrochemical energy storage devices due to their amazing qualities like longer life cycle stability, high specific power and rapid charge/discharge speeds. However, the main barrier to their effective use is the low specific energy compared to batteries. In this scenario, electrode materials with highly efficient electrochemical performance and charge storage capacity are in greater demand for the optimization of superior-performance supercapacitors. As of now, conducting polymers, transition metal oxides, and carbonaceous materials have received the greatest attention as electrode materials.[2,3] Supercapacitors and next-generation battery systems have the potential to contribute to the demand for reliable performance of various smart electronic devices and systems. Supercapacitors offer several benefits over batteries, such as a quicker charge/discharge rate and substantially improved cycle stability. As a result, supercapacitors have been primarily aimed at the replacement of batteries in many energy storage applications. The primary components of supercapacitors are electrode materials, current collectors, separators, and electrolytes. The most important factors that significantly affect the electrochemical performance of supercapacitors are the electrode materials.[4,5] Electrochemical energy storage devices have gained greater relevance owing to the fast rate of the transition from fossil fuel to a clean energy-dependent globe. Due to their remarkable power density, which allows them to store enormous quantities of energy per a given mass and volume, supercapacitors have taken up a significant portion of the market and research space among the many electrochemical energy storage technologies. Supercapacitors like conventional ones, contain two plates, coated with a porous substance (to have a bigger surface), separated by a very narrow insulator, and saturated in an electrolyte. Supercapacitors have the specific property response to improve the power compared to comparable-sized batteries as they offer an enlarged surface area of capacitor plates and a shorter distance between them, leading to enhanced charge storage capacity. The commercially available supercapacitors are majorly made using organic electrolytes and carbon compounds play a primary role.[6] The two major energy storage processes in supercapacitors are pseudo-capacitance and electrochemical double-layer capacitance (EDLC). In EDLC and pseudo-capacitance, respectively, surface redox reactions and ion adsorption store energy. For the effective development of electrode structures for supercapacitors, exceptional electrical conductivity, greater specific surface area, optimal pore size, outstanding stability, and other physicochemical characteristics are highly relevant requisites. Supercapacitors offer a greater energy density than standard dielectric capacitors because the energy storage capacity of a double-layer capacitor is inversely proportional to the thickness. By raising the electrode thickness and eliminating the additives, the energy density of a packed supercapacitor can be effectively increased.[7,8]

Conducting polymers and conducting polymer-based nanocomposites with suitably chosen dispersants have various

property responses favoring electrochemical applications. Polypyrrole (PPy), poly(aniline), poly(paraphenylene), polyacetylene, poly(thiophene) and poly (3-4-ethylenedioxythiophene) are examples of electrically conjugated polymers with numerous electrical applications.[9] The electrical, mechanical, and thermal properties of pristine conductive polymers can be controlled and modified by adding suitable fillers to form composite structures with synergy[10] low power density, poor charging rate, as well as the cracking and fracture of the electrodes are some associated disadvantages of these devices. Efficient energy storage probably entails the use of polymers and their composites. The tunable properties of polymers, when coupled or as hybrids with other materials, make them inevitable energy storage materials. Although the viability of graphene-polymer (Gr-PPy. Due to its simple chemical, electrochemical, or irradiation-based production, tunable electrical conductivity, reduction-oxidation characteristic, and prolonged lifespan at room temperature, polypyrrole (PPy) is one of the most actively researched conjugated polymers[11,12] faster response time (129 s. Composites of conductive polymer with different carbon materials have been successful in the increase of the durability of the polymer composite along with the conductivity and capacitance of the supercapacitors. Three kinds of conducting polymer-based supercapacitors exist. Type I is an asymmetric system in which the same p-dopable conducting polymer is employed on the electrodes of the capacitor. Further, Type II is an asymmetric system with two separate p-dopable conducting polymers, which can be used as electrode materials. Nevertheless, Type III is a symmetric system-based conducting polymer that may be utilized as both n and p-doped electrode material.[13] The present effort addresses the suitability of polypyrrole-coated graphite composite for practically relevant supercapacitor and corrosion inhibition applications. The anticorrosive proper response is studied with reference to mild steel (MS) which is greatly used in different industrial units due to its superior and unique physical and chemical properties linked to precious metals. Also, mild steel metal undergoes corrosion in acid and alkali media. The electrolyte solutions such as HCl, H_2SO_4, and HNO_3 solutions are greatly used for oil well acidizing, descaling and pickling.[14,15] This leads to MS corrosion, which reduces the efficiency of the mild steel.[16] Therefore, the hindrance of mild steel corrosion is very much vital.[17-21] Systematic analysis of the supercapacitor and corrosion inhibition response of polypyrrole/graphite (PPy/G) composites is presented to highlight the multifunctional property response of the synthesized composites.

2. Experimental techniques

2.1 *Materials*

Polypyrrole & graphite nanopowder (analytical grade) are purchased from Sigma-Aldrich Bangalore, Karnataka, India. Pyrrole monomer (analytical grade), Graphite nanopowder (lateral dimension (X and Y) 5-10 μm, mean thickness (z) 3-8 nm, number of layers 3-6, purity > 99%, surface area 180 m^2/g) and ammonium persulphate (analytical grade), were used as obtained.

2.2 *Synthesis of polypyrrole graphite nanocomposites*

The chemical polymerization technique is used to synthesize the PPy and graphite-incorporated PPy nanocomposites. In this typical synthesis process, 0.6 M pyrrole monomer is added into 0.12 M of ammonium persulphate solution with vigorous stirring for 7 hours to maintain the reaction temperature in the range of 0-5 °C to impose polymerization and formation of polypyrrole.[22,23] Synthesized polypyrrole was completely filtered and cleaned with ethanol and distilled water several times to obtain impurity-free polypyrrole. The synthesis of PPy is repeated repeated with the designated weight percentage (10% & 20%) of graphite nanopowder to incorporate them into the polypyrrole system. The resulting composites were (MG1 & MG2 respectively for PPy/G-10%, and PPy/G-20% samples) dried and optimized for the property analysis.

Depending on the precise synthesis method and the quality of the starting materials, the impurities in the PPy-graphite material synthesized can vary. It is important to note, however, that impurities are typically unintended byproducts or residual components of the synthesis process, as opposed to substances that were deliberately added. The pyrrole oligomers, monomer unreacted, residual solvents are removed using water wash, acetonitrile wash and dried.

2.3 *Characterization*

The morphological features of the composites were analyzed using the SEM micrographs (JOEL-JSM-6,380LA, Japan). Structural properties were investigated with the help of powder XRD (PXRD) measurements using a Rigaku 600 miniplex X-ray diffractometer. Fourier transform infrared (FTIR) measurements were performed by FT-IR 4,100 Jasco (Japan) with ATR attachment to analyse the functional group of the composites. Further, the composites were investigated for anticorrosive nature and suitability as supercapacitor electrodes.[24] The anti-corrosive property response on mild steel in 5 M HCl solution was studied by using AAS, potentiodynamic polarization plots, and AC-impedance measurements. The suitability of these composites as supercapacitor electrode structure has been studied using electrochemical Cyclic Voltammetry (CV) and Galvanostatic Charging and Discharging studies (GCD) measurements.

2.4 *Preparation of corrosive solution and specimen metal sample*

Mild steel (MS) with a purity grade of 99% is taken as the specimen to test the corrosion inhibition of the nanocomposites. The compositions of MS are shown in Table 1. 5 M HCl solution is prepared in triple distilled water and kept aside. The MS metal samples were carefully polished to obtain a smooth surface and were submerged in the HCl system with and without composite materials.

Table 1. The chemical components in MS[25]

Element	P	S	Si	C	Mn	Fe
Weight percentage (%)	0.04	0.05	0.1	0.18	0.6	99.03

2.5 *Corrosion inhibition measurements*

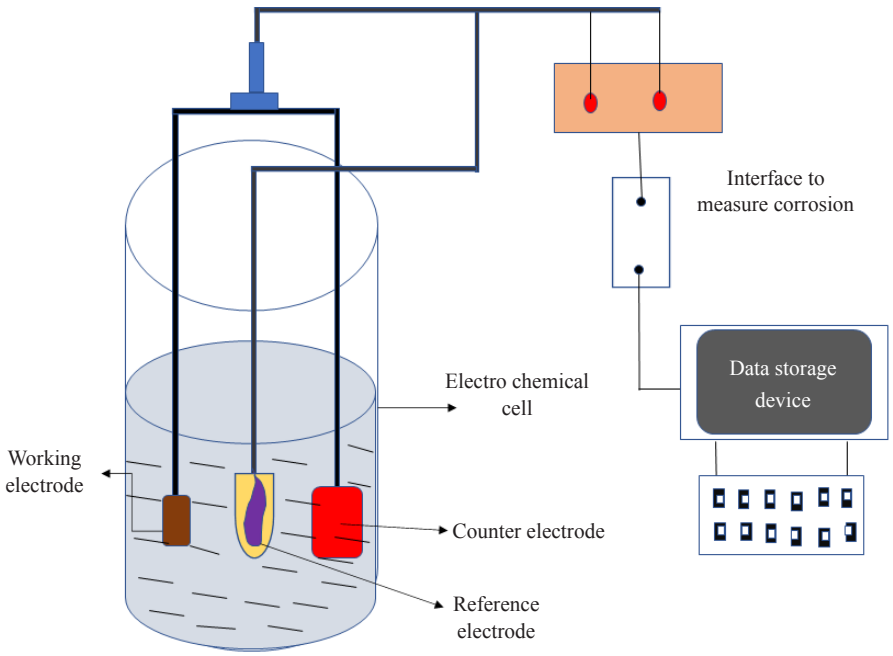

Figure 1. Schematic representation of the 3-electrode system

The effectively polished MS steel specimen was exposed to the corrosive medium and the specified time at ambient temperature, the MS pieces were withdrawn from the test corrosive solution, rinsed and washed with triple distilled water, dried in hot air, and weighed. The protection efficiency is calculated as per the widely accepted standard method from literature.[26] Three electrode systems (working electrode (MS), reference electrode (saturated calomel electrode and auxiliary electrode is platinum)) of the CHI 660 C instrument were used for the examination of the inhibitory properties of the polymer. Figure 1 illustrates the schematic of three electrode system to analyze the corrosion inhibition properties. In the present investigation, samples were characterized in the potential range of -200 to +200 mV with a 0.01 V/s sweep rate for the Tafel plot measurement. The inhibition efficiency [IE] calculations were carried out using the following Equation 1.

$$IE = \frac{\left(\left[\text{MS corrosion density value in unprotected system} - \text{MS corrosion density value in unprotected system}\right]\right)}{\text{MS corrosion density value in unprotected system}} \times 100 \quad (1)$$

3. Results and discussions

3.1 *Structural and morphological characteristics*

3.1.1 *PXRD measurements*

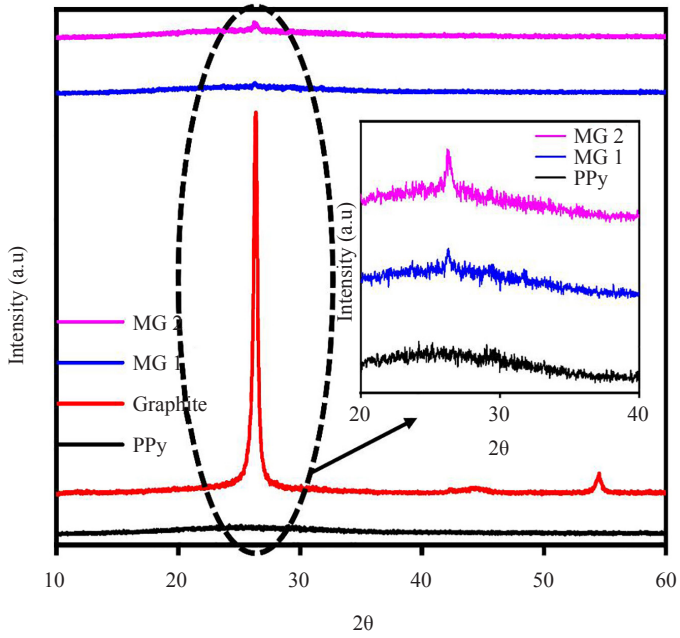

Figure 2. PXRD patterns of the PPy, Graphite, MG1, and MG2 samples

The structural investigations were carried out using powder X-ray diffraction studies. Figure 2 depicts the PXRD patterns of PPy, Graphite, and MG1 and MG2 hybrid composite materials. From the Figure 2, it is evident that the pure PPy exhibits a typical amorphous phase which is the characteristic nature of semiconducting PPy samples. The occurrence of the broad amorphous peak can be attributed to the polymer chain scattering of the PPy matrix. The occurrence of the sharp peak at 26° is the signature peak of graphite. As the graphite is incorporated into the PPy matrix, the composite materials reveal a peak at 26°, further, the intensity of the composites was increased as the graphite

doping percentage increased. The composite's X-ray diffractograms clarify the effective incorporation of the dispersant graphite into the polypyrrole matrix.

3.1.2 *FTIR spectra analysis*

The existence of functional groups in pristine PPy, graphite, and PPy/G nanocomposites (MG1, and MG2) was analysed by using FT-IR spectrum studies. Figure 3 depicts the FT-IR spectra of pristine PPy and PPy/G nanocomposites (MG1, and MG2). From the obtained absorption spectra a peak corresponding to 1,557 cm^{-1} can be recognized as C = C stretching mode. The absorption peak corresponding to 579 cm^{-1} can be ascribed to C-N stretching vibration. The absorption peaks corresponding to 1,043 and 1,190 cm^{-1} are attributed to the C-H deformation and C-C stretching. Further, the absorption peak corresponding to 921 cm^{-1} can be assigned to C-C out of plane deformation. The corresponding peaks observed from the PPy samples match with the characteristic vibrations of the PPy, which confirms the structural effectiveness of the synthesized polypyrrole (PPy). The absorption peaks of MG1 and MG2 composites are well matching with the pristine PPy. The composite spectra have shown a small shift in absorption peaks confirming the incorporation of graphite into the polypyrrole (PPy) matrix and infer that the PPy matrix is physically modified without altering the functional bonds as correlated by the X-ray diffractogram.

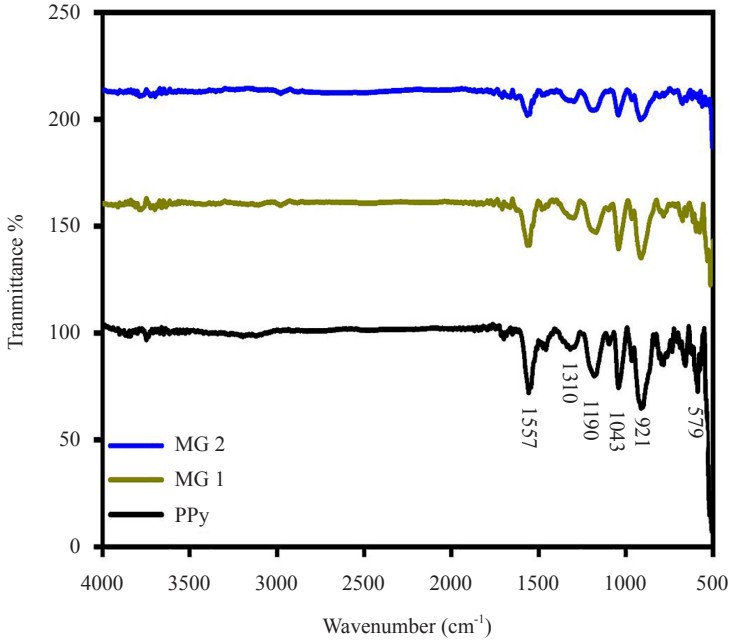

Figure 3. FT-IR patterns of the PPy, MG1 and MG2 samples

3.1.3 *SEM analysis*

SEM images of PPy, Graphite, MG1, and MG2 are shown in Figure 4. From the SEM images, it was clearly revealed the changes in the structural morphologies of the composite materials. Pristine PPy and Graphite SEM morphologies revealed granular structure, further, the graphite-incorporated PPy depicts dense morphology with modified phase boundaries. The arrangement of these two components is depicted in the structural diagram of a polypyrrole graphite nanocomposite. Imagine a lattice-like structure consisting of a graphite matrix that forms a three-dimensional network. Polypyrrole particles are evenly embedded or dispersed throughout this matrix.

Polypyrrole graphite nanocomposites are composed of polypyrrole particles dispersed in a graphite matrix. This hybrid structure combines the electrical conductivity and stability of graphite with the unique properties of polypyrrole, allowing for a vast array of applications in electronics, energy storage, and sensing. The physical changes observed are

important for the various property responses and could be attributed to the successful incorporation of Graphite into the PPy[12] optical and electrical properties. Structural and morphological studies were performed using powder X-ray diffraction, Fourier transform infrared spectroscopy, scanning electron microscopy and the effect of graphite on the properties of PPy is elaborated in detail. Further, the electrical measurements were carried using dielectric analyzer. Dielectric behavior of the composites was also compared with the PPy and graphite and confirmed the dependency of graphite on PPy/graphite nanocomposites. The EMI shielding response of PPy/graphite nanocomposites were measured in the microwave frequency range from 12 to 18 GHz (Ku band).

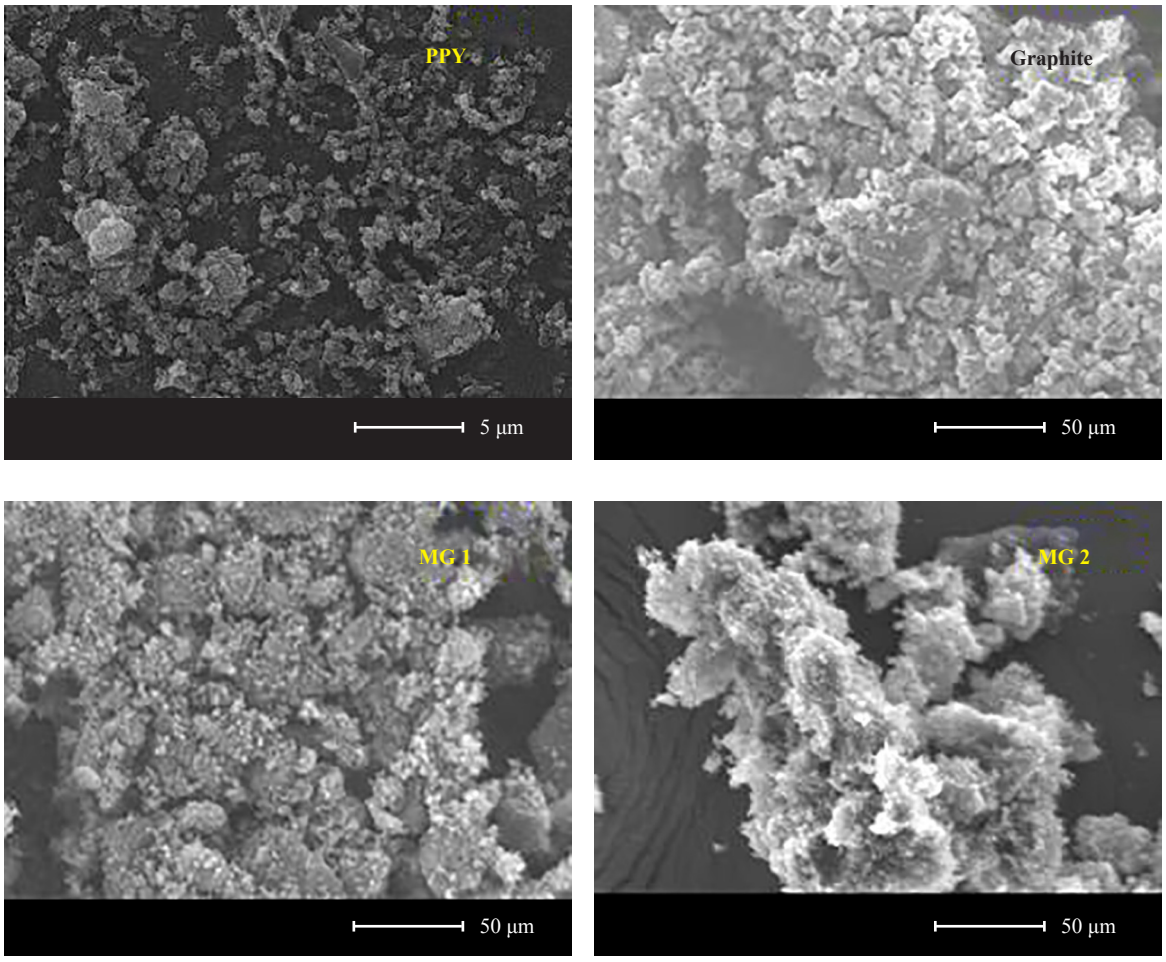

Figure 4. SEM micrographs of PPy, graphite, MG1, and MG2 samples

3.2 *Evaluation of corrosion inhibition*

3.2.1 *AAS technique*

The effect of corrosion on MS in an HCl solution was explored with the help of AAS measurements. The material stability of the protective film was also studied at different concentrations part of polymers. The variation in the amount of iron dissolved and protection efficiency with respect to inhibitor concentration is shown in Table 2. It was observed that protection (inhibition) efficiency increases with an increase in the dose of polymer nanocomposite.[27] The observed protective action of green inhibitors can be explained due to the interaction of polymer species with MS surface in acid media as shown in Figure 5. The protective film formation limits the disintegration process by limiting MS corrosion sites. Hence, as the polymer nanocomposition dose increases the protection efficiency increases and a decrease in the iron is observed.

Table 2. AAS results

Concentration of inhibitor (mg/L)	Amount of MS dissolved in acid solution (mg)	Surface coverage (Θ)	Inhibition efficiency (%)
Bare	87		
0.5	43	0.5057	50.574
1.0	31	0.6436	64.367
1.5	19	0.781	78.160
2.0	10	0.885	88.505
2.5	7	0.919	91.954

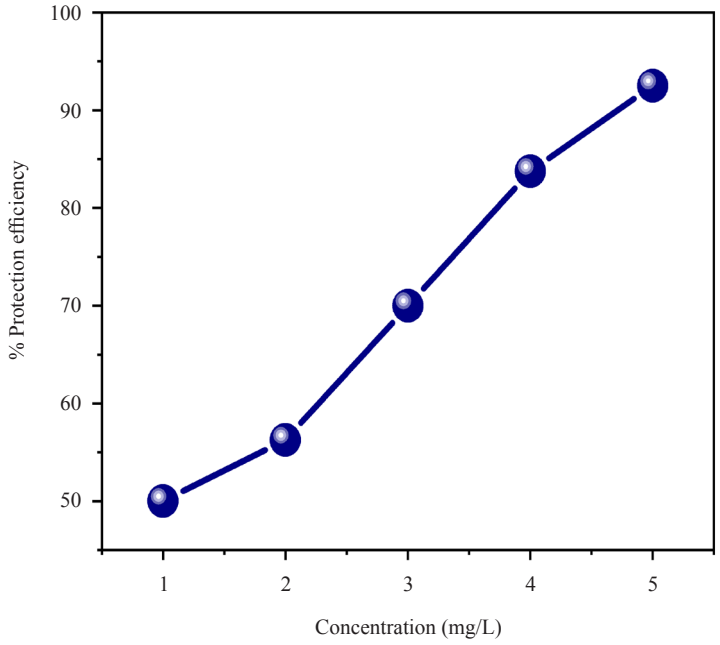

Figure 5. AAS of PPy/G composites

3.2.2 *Tafel plot (potentiodynamic polarization) and impedance measurement*

The kinetics of MS corrosion can be interpreted using Tafel plots and impedance measurements. Figure 6 depicts the Tafel and impedance plots of MS corrosion in HCl media. The corrosion potential (E_{corr}), Tafel anodic and cathodic (β_a and β_c), corrosion current density (i_{corr}), and protection efficiency (%) of the inhibitor are shortened in Table 3. In the present investigation, it is also witnessed that the polymer nanocomposite remarkably decreased MS corrosion current density (decrease in the MS corrosion rate). An increase in the amount of polymer nanocomposite results in superior resistance to the corrosion of MS in an acid environment, illustrating that Polymer nanocomposite possesses favorable properties. This result provides a hint that; a tenacious layer is generated by the polymer nanocomposite. The presence of an adsorbed invisible layer efficiently blocks the annihilation of corrosive ions (from both acid environments). Apparently, the interaction that exists between the adsorbed inhibitor molecule and the MS surface is strong and sufficient to prevent the disintegration process. In the present investigation, the difference in the E_{corr} values (between

bare and protected systems) is more than 85 mV in an acid environment. However, no measurable difference in anodic and cathodic Tafel slope values. The presence of polymer nanocomposite affects both anodic and cathodic Tafel slopes, revealing that green inhibitors act like a mixed type toward the MS corrosion process in acid media.[27,28] Nyquist plot results are displayed in Table 4 and Figure 7. From this, it is obvious that charge transfer resistance values increase with an increase in the polymer nanocomposite concentration is a clear indication of the corrosion inhibition property of polymer nanocomposite on MS in 5 M HCl solution system. From the table, it is clear that, the charge transfer process principally controls the metal dissolution process by enhancing the double-width layer as stated by the Helmholtz model. This decreases the direct contact between metal and corrosive solution.[29] The area of the depressed semicircle is high in the presence of polymer nanocomposite as compared to the blank system. This shows that adsorption increases with an increase in the polymer nanocomposite concentration.

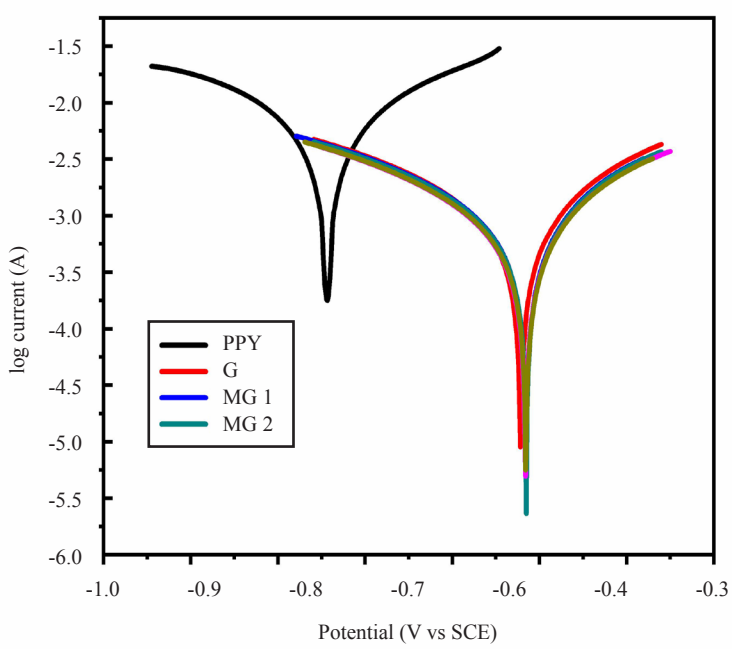

Figure 6. Tafel plots and impedance plots without and with polymer

Table 3. Tafel plot results

Concentration (mg/L)	Corrosion potential (mV)	Cathodic Tafel slope (V/dec)	Anodic Tafel slope (V/dec)	Corrosion current (A)	PE (%)
Bare	-743	4.480	4.908	6.234×10^{-3}	
0.5	-522	4.800	5.701	8.001×10^{-4}	87.165
1.0	-515	5.001	5.600	7.600×10^{-4}	87.808
1.5	-515	5.000	5.7	7.3×10^{-4}	88.225
2.0	-516	5.069	5.727	6.7×10^{-4}	89.19
2.5	-516	5.008	5.749	6.668×10^{-4}	89.354

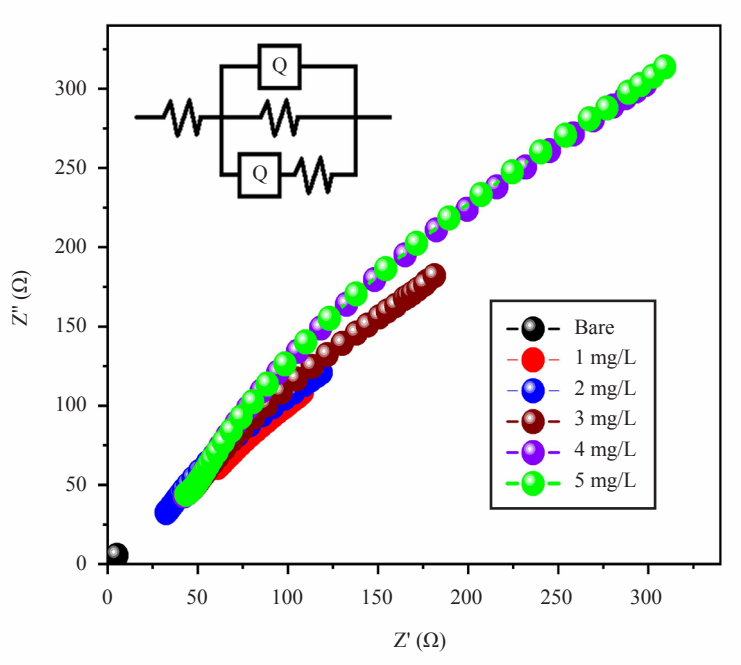

Figure 7. Nyquist plot without and with inhibitor

Table 4. Impedance parameters

Concentration (mg/L)	Charge transfer resistance (Ω)	n	y^{-2}	PE (%)
Bare	5.8	0.70	9.9×10^{-3}	
0.5	122	0.84	1×10^{-4}	95.24
1.0	141	0.89	1×10^{-4}	95.88
1.5	256	0.89	1×10^{-4}	97.773
2.0	291	0.91	6.6×10^{-4}	98.006
2.5	319	0.90	4.7×10^{-4}	98.181

3.2.3 *Scanning electron microscopy (SEM) measurements*

The surface morphology of MS in the presence and absence of the polymer was studied by using SEM technique. The MS surface study was carried out by an SEM technique without and with polymer nanocomposite for MS metal in an HCl solution. Figure 8a is the SEM image of the MS surface without any inhibitor treatment. The micrographs revealed the presence of pores and cracks on the surface of MS, which can be interpreted as the direct attack from corrosive ions on the MS surface in an acid medium. Figure 8b revealed the enhanced MS surface with less quantities of cracks and pores on the MS metal surface. The different surface morphology (smooth layer) in the protected acid medium can be due to the adsorption of electron-rich elements on the metal surface.

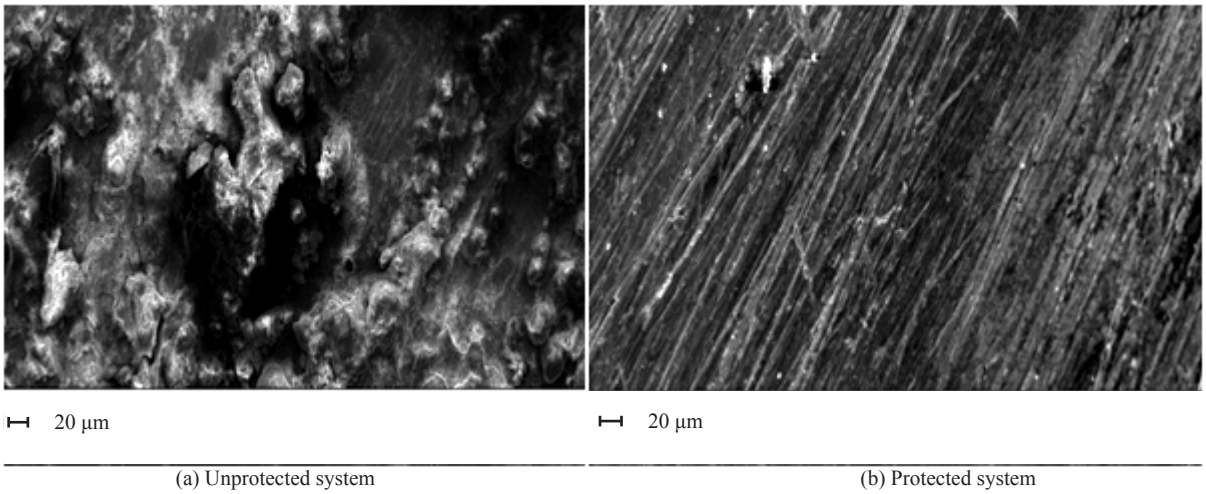

Figure 8. SEM images of MS (a) without MG and (b) with MG nanocomposites inhibitor

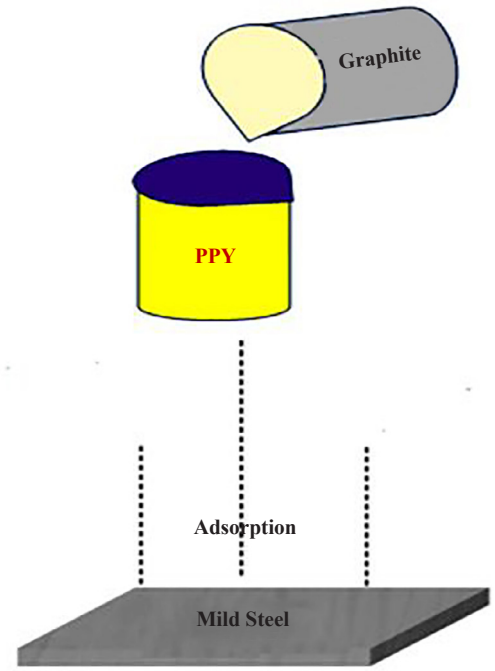

Figure 9. Adsorption of PPy/G nanocomposites on MS in 5 M HCl solution

The mild steel corrosion in 5 M HCl solution was studied without and with PPy/Graphite nanocomposites. The presence of PPy/Graphite nanocomposite on the mild steel forms a barrier layer, which prevents the direct contact between 5 M HCl and MS. The electron-rich species in the PPy/Graphite nanocomposites strongly adsorbed on the MS in 5 M HCl solution. The Tafel plots results reveal that there is no significant variation in the anodic and cathodic Tafel slope values. The adsorption of PPy/Graphite nanocomposites shows the mixed corrosion inhibition property. The schematic representation of adsorption of PPy/Graphite nanocomposites on MS in 5 M HCl is shown in Figure 9. Mixed type of adsorption confirmed by electrochemical studies.

3.3 *Supercapacitor response analysis*

3.3.1 *Cyclic voltammetry*

Cyclic Voltammetry studies have been done for ppy/Graphite nanocomposite and are shown in Figure 10. rectangular shape curves were obtained showing oxidation and reduction in the material for a scan rate of 30 mV for a potential range of -0.6 to 0.4 V indicating the effect of Graphite in the PPy matrix. The area enclosed in the CV curve is directly proportional to capacitance and it is observed that the MG2 sample encloses more area under the CV curve which indicates the presence of Graphite in the sample which enhances the capacitance of the composite.[30] The reversible existence of the electrode (anodic oxidation and cathodic reduction) in a suitable electrolyte is determined by using cyclic voltammetry, and the basic capacitance (C) changes with the scan rate. The CV test of the PPy, MG1, and MG2 electrode materials was performed at the sweep rate of 30 mV within the potential ranges of -0.6-0.4 V. Figure 10. shows the typical CV curve of MG2 revealing a symmetric rectangular shape indicating the effects of graphite in the PPy matrix. The integral area of the MG2 sample was much greater than the other and the sample showed the best capacitance.

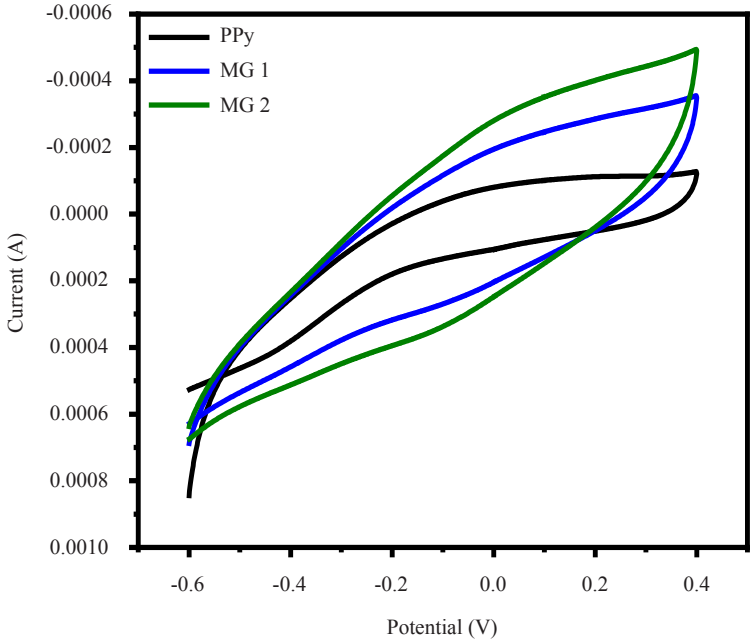

Figure 10. CV plots of pure PPy and PPy/Graphite nanocomposites

3.3.2 *Galvanometric charging and discharging (GCD)*

The charge/discharge curves of PPy nanocomposites are shown in Figure 11. GCD curves of electrode samples show a quasi-symmetric capacitive characteristic. These curves show the performance of the visible pseudo capacitance as they deviate from the correct line position. Release time decreased with graphite to add to the PPy matrix. PPy has shown an almost identical environment with high ratings. PPy release time was significantly longer than MG1 and MG2 samples, which indicated that the MG2 sample showed high strength, and this result was consistent with the CV test result.

PPy has a charging time of 0 to 4 s and a discharge time of 4 to 8 s. MG1 has a charging time of 0 to 5 s and a discharge time of 5 to 10 s. MG2 has a charge time of 0 to 8 s and a discharge time of 8 to 14 s. From these observations from the GCD curve it is evident that compared to ppy the ppy/graphite composites GM1 and GM2 are showing more discharge time which proves the potential of these composites to use for supercapacitor applications.[31]

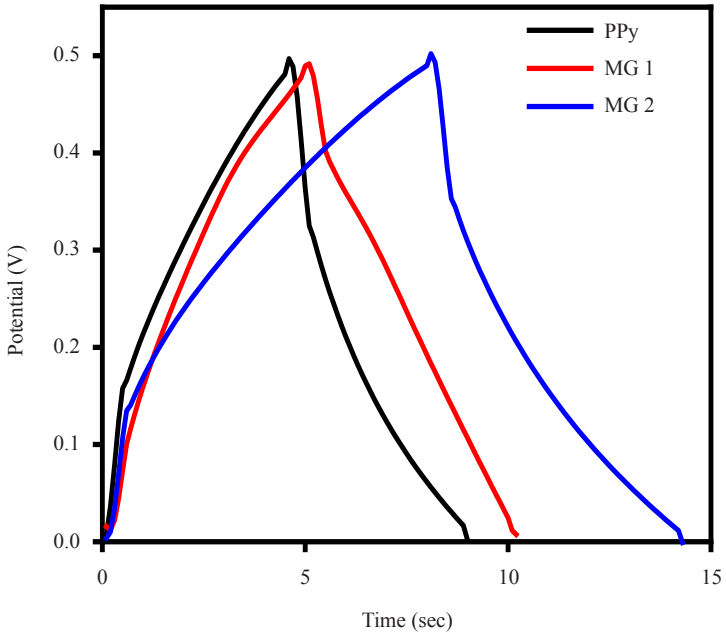

Figure 11. Galvanostatic charge/discharge plot of pure PPy and PPy/graphite nanocomposites

4. Conclusions

This work demonstrates the possible optimization of cost-effective and anticorrosive supercapacitor electrodes-based PPy/G nanocomposites. The structure/morphological properties and characteristics of the composites were supported by PXRD, FTIR, and SEM measurements. The composite samples have exhibited good corrosion inhibition on the MS surface in an acid medium. The obtained results from the Tafel plot, AAS and impedance measurements revealed the concentration-dependent inhibition of the PPy composite on the MS metal through the adsorption mechanism (both physical and chemical adsorption). The investigated polymer inhibitor the MS corrosion in HCl solutions via mixed mode. Surface analysis by SEM technique also hints at the protective behavior of the polymer. Both the CV and GCD responses have shown promising results for PPy/G composites indicating the potential and the possible prospects towards the optimization of anticorrosive electroactive material for supercapcitor applications.

Conflict of interest

The authors confirm that they have no financial or interpersonal conflicts that may have looked to have influenced the research presented in this study.

Acknowledgements

The authors are grateful for the help and encouragement they have received from the principal and administration of Vemana Institute of Technology in Koramangala, Bangalore, and the management of PES University-Electronic City, Bangalore.

References

[1] Alcaraz-espinoza, J. J.; Oliveira, H. P. D. Flexible supercapacitors based on a ternary composite of polyaniline/polypyrrole/graphite on gold coated sandpaper. *Electrochim. Acta* **2018,** *274*, 200-207. https://doi.org/10.1016/j.electacta.2018.04.063.

[2] Madhusudhan, C. K.; Mahendra, K.; Madhukar, B. S.; Somesh, T. E.; Faisal, M. Multifunctional polypyrrole/multi-walled carbon nanotube composite material: Dielectric, humidity sensing and broadband EMI shielding properties. *Polymer Science, Series B* **2021,** *63*(3), 280-290. https://doi.org/10.1134/S156009042103009X.

[3] Kulandaivalu, S.; Naim, M.; Azahari, M.; Hawa, N.; Azman, N. Ultrahigh specific energy of layer by layer polypyrrole/graphene oxide/multi-walled carbon nanotube|polypyrrole/manganese oxide composite for supercapacitor. *J. Energy Storage* **2020,** *28*, 101219. https://doi.org/10.1016/j.est.2020.101219.

[4] Oskueyan, G.; Mansour, M.; Mojtaba, L. Fabrication of polyaniline-carrot derived carbon dots/polypyrrole-graphene nanocomposite for wide potential window supercapacitor. *Carbon Lett.* **2020,** *31*(2), 269-276. https://doi.org/10.1007/s42823-020-00162-w.

[5] Yuksel, R.; Uysal, N.; Aydinli, A.; Unalan, H. E. Paper based, expanded graphite/polypyrrole nanocomposite supercapacitors free from binders and current collectors. *J. Electrochem. Soc.* **2018,** *165*(2), A283-A290. https://doi.org/10.1149/2.1051802jes.

[6] Samukaite-Bubniene, U.; Valiūnienė, A.; Bucinskas, V.; Genys, P.; Ratautaite, V.; Ramanaviciene, A.; Aksun, E.; Tereshchenko, A.; Zeybek, B.; Ramanavicius, A. Towards supercapacitors: Cyclic voltammetry and fast fourier transform electrochemical impedance spectroscopy based evaluation of polypyrrole electrochemically deposited on the pencil graphite electrode. *Colloids Surfaces A Physicochem. Eng. Asp.* **2021,** *610*, 125750. https://doi.org/10.1016/j.colsurfa.2020.125750.

[7] Kandasamy, S. K.; Kandasamy, K. Recent advances in electrochemical performances of graphene composite (graphene-polyaniline/polypyrrole/activated carbon/carbon nanotube) electrode materials for supercapacitor: A review. *J. Inorg. Organomet. Polym. Mater.* **2018,** *28*(3), 559-584. https://doi.org/10.1007/s10904-018-0779-x.

[8] Kulandaivalu, S.; Suhaimi, N.; Sulaiman, Y. Unveiling high specific energy supercapacitor from layer-by-layer assembled polypyrrole/graphene oxide|polypyrrole/manganese oxide electrode material. *Sci. Rep.* **2019,** *9*(1), 1-10. https://doi.org/10.1038/s41598-019-41203-3.

[9] Madhusudhan, C. K.; Mahendra, K.; Raghavendra, N.; Revanasiddappa, M.; Faisal, M. Corrosion-resistant polypyrrole-banana carbon (PPy-BC) nanocomposites for protection against electromagnetic interference: A green approach. *J. Mater. Sci. Mater. Electron.* **2022,** *33*, 1366-138. https://doi.org/10.1007/s10854-021-07466-1.

[10] Folorunso, O.; Hamam, Y.; Sadiku, R.; Ray, S. S.; Adekoya, G. J. Synthesis methods of borophene, graphene-loaded polypyrrole nanocomposites and their benefits for energy storage applications: A brief overview. *FlatChem* **2021,** *26*, 100211. https://doi.org/10.1016/j.flatc.2020.100211.

[11] Guettiche, D.; Mekki, A.; Lilia, B.; Fatma-Zohra, T.; Boudjellal, A. Flexible chemiresistive nitrogen oxide sensors based on a nanocomposite of polypyrrole-reduced graphene oxide-functionalized carboxybenzene diazonium salts. *J. Mater. Sci. Mater. Electron.* **2021,** *32*(8), 10662-10677. https://doi.org/10.1007/s10854-021-05721-z.

[12] Madhusudhan, C. K.; Mahendra, K.; Madhukar, B. S.; Somesh, T. E.; Faisal, M. Incorporation of graphite into iron decorated polypyrrole for dielectric and EMI shielding applications. *Synth. Met.* **2020**, *267*, 116450. https://doi.org/10.1016/j.synthmet.2020.116450.

[13] Konwer, S.; Boruah, R.; Dolui, S. K. Studies on conducting polypyrrole/graphene oxide composites as supercapacitor electrode. *J. Electron. Mater.* **2011,** *40*(11), 2248-2255. https://doi.org/10.1007/s11664-011-1749-z.

[14] Raghavendra, N.; Bhat, J. I. Anticorrosive property of arecanut seed extracts on 63,400 type al in 0.1 m NaOH solution. *Res. J. Chem. Environ.* **2018,** *22*(1), 14-24.

[15] Raghavendra, N.; Ishwara Bhat, J. Inhibition of al corrosion in 0.5 m HCl solution by areca flower extract. *J. King Saud Univ.-Eng. Sci.* **2019,** *31*(3), 202-208. https://doi.org/10.1016/j.jksues.2017.06.003.

[16] Raghavendra, N. *An Investigation on the Effect of Areca Plant Extracts as Corrosion Inhibitors for Aluminum, Mild Steel and Copper in Acid and Alkali Media*; Mangalore University, 2018.

[17] Raghavendra, N. Green compounds to attenuate aluminum corrosion in hcl activation: A necessity review. *Chem. Africa* **2020,** *3*(1), 21-34. https://doi.org/10.1007/s42250-019-00114-6.

[18] Raghavendra, N.; Bhat, J. I. Protection of aluminium metal in 0.5 m HCl environment by mature arecanut seed extracts: A comparative study by chemical, electrochemical and surface probe screening techniques. *J. Phys. Sci.* **2018,** *29*(1), 77-99. https://doi.org/10.21315/jps2018.29.1.6.

[19] Raghavendra, N. Areca plant extracts as a green corrosion inhibitor of carbon steel metal in 3 m hydrochloric acid: Gasometric, colorimetry and atomic absorption spectroscopy views. *J. Mol. Eng. Mater.* **2018,** *6*, 1850004. https://

doi.org/10.1142/s2251237318500041.
[20] Maruthi, N.; Faisal, M.; Raghavendra, N.; Prasanna, B. P.; Manohara, R.; Revanasiddappa, M. Anticorrosive Polyaniline-Coated Copper Oxide (PANI/CuO) nanocomposites with tunable electrical properties for broadband electromagnetic interference shielding. *Colloids Surfaces A Physicochem. Eng. Asp.* **2021,** *621*, 126611. https://doi.org/10.1016/j.colsurfa.2021.126611.
[21] Raghavendra, N.; Bhat, J. I. An environmentally friendly approach towards mitigation of al corrosion in hydrochloric acid by yellow colour ripe arecanut husk extract: introducing potential and sustainable inhibitor for material protection. *J. Bio-Tribo-Corrosion* **2018,** *4*(1). https://doi.org/10.1007/s40735-017-0112-1.
[22] Konwer, S.; Dolui, S. K. Synthesis and characterization of polypyrrole/graphite composites and study of their electrical and electrochemical properties. *Mater. Chem. Phys.* **2010,** *124*(1), 738-743. https://doi.org/10.1016/j.matchemphys.2010.07.049.
[23] Chandrasekhar, P. *Conducting Polymers, Fundamentals and Applications: A Practical Approach*; Springer New York, NY, 1999.
[24] Yadav, D. K.; Quraishi, M. A.; Maiti, B. Inhibition effect of some benzylidenes on mild steel in 1 m HCl: An experimental and theoretical correlation. *Corros. Sci.* **2012,** *55*, 254-266. https://doi.org/10.1016/j.corsci.2011.10.030.
[25] Raghavendra, N.; Bhat, J. I. Application of green products for industrially important materials protection: An amusing anticorrosive behavior of tender arecanut husk (green color) extract at metal-test solution interface. *Measurement* **2018,** *135*, 625-639. https://doi.org/10.1016/j.measurement.2018.12.021.
[26] Maruthi, N.; Faisal, M.; Raghavendra, N.; Prasanna, B. P.; Manohara, S. R.; Revanasiddappa, M. Promising EMI shielding effectiveness and anticorrosive properties of PANI-Nb_2O_5 nanocomposites: Multifunctional approach. *Synth. Met.* **2021,** *275*, 116744. https://doi.org/10.1016/j.synthmet.2021.116744.
[27] Raghavendra, N. Expired lorazepam drug: A medicinal compound as green corrosion inhibitor for mild steel in hydrochloric acid system. *Chem. Africa* **2019,** *2*(3), 463-470. https://doi.org/10.1007/s42250-019-00061-2.
[28] Hublikar, L. V.; Ganachari, S. V.; Raghavendra, N.; Banapurmath, N. R.; Patil, V. B.; Khan, T. M. Y.; Badruddin, I. A. Biogenesis of silver nanoparticles and its multifunctional anti-corrosion and anticancer studies. *Coatings* **2021,** *11*(10), 1215. https://doi.org/10.3390/coatings11101215.
[29] Hegde, M.; Nayak, S. P.; Raghavendra, N. Microwave-assisted extraction of swietenia macrophylla fruit shell and its application in corrosion inhibition for mild steel in 0.5 m HCl pickling environment. *Sādhanā* **2023,** *48*(1), 10. https://doi.org/10.1007/s12046-022-02066-z.
[30] Raj, T. N. V.; Hoskeri, P. A.; Muralidhara, H. B.; Manjunatha, C. R.; Kumar, K. Y.; Raghu, M. S. Facile synthesis of perovskite lanthanum aluminate and its green reduced graphene oxide composite for high performance supercapacitors. *J. Electroanal. Chem.* **2020,** *858*, 113830. https://doi.org/10.1016/j.jelechem.2020.113830.
[31] Raj, T. N. V.; Hoskeri, P. A.; Hamzad, S.; Anantha, M. S.; Joseph, C. M.; Muralidhara, H. B.; Kumar, K. Y.; Alharti, F. A.; Jeon, B.-H.; Raghu, M. S. Moringa oleifera leaf extract mediated synthesis of reduced graphene oxide-vanadium pentoxide nanocomposite for enhanced specific capacitance in supercapacitors. *Inorg. Chem. Commun.* **2022,** *142*, 109648. https://doi.org/10.1016/j.inoche.2022.109648.